PORE-LEVEL VALIDATION OF REPRESENTATIVE PORE NETWORKS OBTAINED FROM MICRO-CT IMAGES

J. Y. Arns[1], A. P. Sheppard[2], C. H. Arns[2], M. A. Knackstedt[1,2], A. Yelkhovsky[1], W. V. Pinczewski[1]

(1) School of Petroleum Engineering, University of New South Wales, Sydney, Australia
(2) Applied Maths, RSPhysSE, Australian National University, Canberra, Australia

This paper was prepared for presentation at the International Symposium of the Society of Core Analysts held in Calgary, Canada, 10-12 September, 2007

ABSTRACT

We test the accuracy of pore network models generated from microtomographic images by comparing computations of permeability and wetting fluid continuity based on the images and network models extracted from the images. The comparisons are made for three rock-types including two clastic rocks (consolidated and unconsolidated) and one outcrop carbonate. We describe the network extraction procedure and note the non-unique aspects of the resultant networks and the effect which this has on predictions of permeability. Permeabilities are found to be in very good agreement for large image volumes (>10,000 pores). At a local scale we compare the flow rates within individual pores for the image based computations with those for the network. Whilst there is considerable scatter in the data, the overall trends are similar. We also question the merits of the usual network model assumptions that every pore and throat in the network has a uniform cross-sectional shape, determined from an equivalent shape factor, and that corner wetting fluid remain continuous throughout the network. An image based investigation of the connectivity of the crevice wetting phase shows that corner wetting phase becomes increasingly disconnected as the wetting phase saturation is reduced.

INTRODUCTION

Pore network simulations have become established tools for the simulation of two-phase fluid flow in porous materials. The guiding idea is that, in the context of capillary dominated flow, the pore space can be naturally discretised into subvolumes separated at the locally narrowest constrictions. The subvolumes and the constrictions can then be identified with the nodes (pore bodies) and links (pore throats) of a complex 3D network. The movement of a fluid-fluid interface through a link or node in the network is governed by the relationship between the capillary pressure, wettability and the local channel cross-section geometry. This method implicitly assumes that every pore space can be well characterised by the simplified geometry of a ball-and-stick network, and that this network is unique. Both of these assumptions are incorrect, as there are many geometries that cannot be well represented by any single network. Network extraction therefore

remains an inexact process in which one must find a compromise that best balances various competing goals. We illustrate these difficulties with specific examples for clastic samples generated via X-ray microtomography (micro-CT).

In this paper we consider the accuracy of pore network models generated from three clastic and carbonate samples imaged using micro-CT by direct comparison with voxel-based simulation data for the same images. Arns et al. (2004) show that the image based LB (lattice Boltzmann) model is a well-proven technique for high permeability (~10mD) rocks. We compare single phase permeabilities for image and network based simulations. We observe very good agreement for the single phase permeability for large volumes (equivalent to >10,000 pores), but much poorer agreement for smaller image volumes. At a local scale we consider the accuracy of the assumption of a single equivalent channel cross-section geometry on fluid configurations and compare the local flow rates within individual pores. We compute drainage fluid distributions directly on the 3D images and determine the connectivity of the wetting fluid as a function of saturation. In contrast to the implicit assumption in multi-phase network models that the wetting fluid is always continuous as a result of corner geometry, we find that corner wetting phase becomes increasingly disconnected with decreasing wetting fluid saturation. The implications of this to electrical resistivity are discussed.

Table 1. *Characteristics of the reconstructed images with porosity as measured from porosimetry and from the image data. Porosity could not be accurately measured for the unconsolidated sand pack.*

Type	Image size (voxels)	Voxel Size (μm)	Porosity (Experiment)	Porosity (Image)
Castlegate Sand	960 x 1096 x 1560	5.6	27.2%	25.8%
Unconsolidated	1420 x 1420 x 1860	9.1		31.5%
Limestone	1696 x1688 x 1936	3.0	45.1%	43.8%

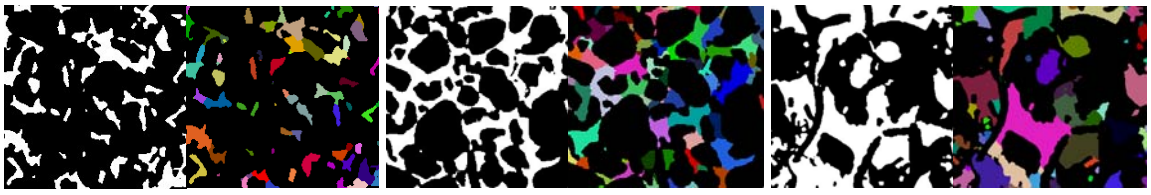

(a) ***(b)*** ***(c)***

Fig. 1: *A pair of images, phase-separated (left) and pore partitioned (right), showing sections of Castlegate sandstone (a), the unconsolidated sand pack (b) and Mt. Gambier limestone (c).*

ROCK TYPES

Three rock types are considered in this paper. The first is Castlegate sandstone, a fine to medium grained high porosity quartz sandstone with small clay fractions. The second sample is an unconsolidated fluvial quartz sediment removed from an active riverbed. The third is a highly porous and permeable quarried fossiliferous outcrop limestone from

Mt. Gambier, Australia. The limestone is composed of readily identifiable coral fossil fragments with a minor amount of coarse sparry calcite. All images were acquired at 2048^3 voxels. Fig. 1 shows small subsets of phase separated images of the three samples. Additional data is summarized in Table 1.

NETWORK REPRESENTATION: METHODOLOGY AND AMBIGUITIES

The first major task in constructing a network representation of a pore space is to partition the pore space into subvolumes - pore bodies - separated at locally narrowest constrictions. In the context of capillary dominated flow it is reasonable to define a constriction's size as the radius of the largest sphere that can pass through it. This measure is easily calculated using the Euclidean distance transform (EDT) of the pore space. We use the EDT to identify pore bodies using a three-step process (Sheppard et al., 2006). First, we identify pore body centres as junctions of the EDT-based medial axis (Lindquist et al 2000). Second, we use the centres as seed points for a watershed partitioning (Russ 2007). Third, we merge pore-bodies together if the constriction between them is judged to be insufficiently narrow.

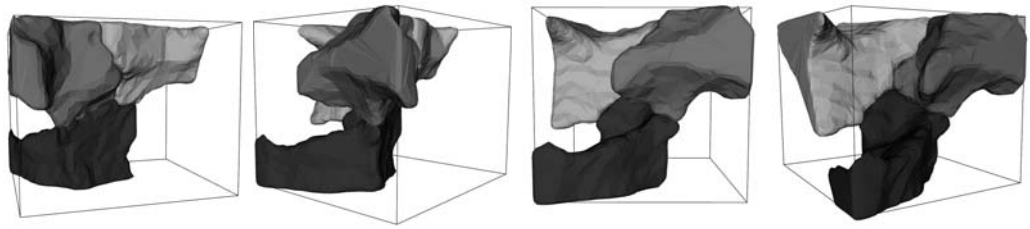

(a) (b) (c) (d)

Fig. 2: *Four different perspectives of a pore geometry in the Castlegate sample that has an ambiguous network representation. Three pore bodies are present; to aid visualization each is shaded a different colour. At the centre of the structure, where the pore bodies meet, is a relatively thin plate-like feature. Since this feature can be considered both a constriction and a junction, it cannot easily be represented by a network.*

The only significant free parameter in pore partitioning controls the amount of pore merging that is performed. This uncertainty is unavoidable; the decision on whether a particular subvolume should be represented by a single pore body or by two distinct pores separated by a throat will be somewhat arbitrary for some subvolumes in any sufficiently complex pore space - even sphere packs (Sheppard et al. 2006). Since pore merging produces different networks, it is possible to create a number of different networks from a single image that have very different numbers of pores, pore and throat sizes and coordination numbers. However, it is reasonable to expect that these networks will all exhibit similar transport properties and this is verified by results presented later in the paper.

Although the pore-partitioning process is fundamentally well defined, it will not perform well on all materials, since there are many geometries that are inherently difficult to

represent by a network. Difficult pore spaces often exhibit plate-like structure, and particular difficulties arise when the junctions of tunnels - the traditional locations of pore bodies - are actually constrictions. This scenario is illustrated in Fig. 2. Far from being a rare pathological case, this occurs to a significant degree in all real porous rocks which we have studied. The usual consequence of these non-ideal geometries is that the boundaries between pores – i.e. the throats - are not completely isolated, but may touch each other. One can measure this aspect of the quality of a partitioning by calculating the fraction of the total throat perimeter length that is "bad", i.e. in contact with other throats (Sheppard et al 2005). For the 3 rock types considered here, the Castlegate sandstone had 11% bad perimeter, the unconsolidated sand 15% and the limestone 27%.

Fig 3: *Images illustrating pore and throat partitioning for a small 2D section of the Castlegate data set. All functions shown here were calculated on the full 3D sample. (a) Euclidean distance transform (EDT) – light regions represent bigger distances; (b) covering radius transform (CRT); (c) watershed pore partitioning – region boundaries are the watersheds of the EDT; (d), (e) two possible valid allocations of volume to throats. Note that in (e) the throats touch one another. In three dimensional structures this is unavoidable.*

In contrast to the unambiguous definition of constrictions, there is no clear method for further partitioning the pore space in order to allocate volume to throats. There are a number of equally acceptable alternatives to positions for the boundary line dividing the pore body from the throat, often leading to large differences in the resulting throat volumes. Unfortunately, fluid saturations, and therefore saturation dependent transport properties, are sensitive to throat volumes. It therefore remains an important challenge to design both network models and network extraction tools that minimize this uncertainty.

One elegant way is shown in Fig. 3. To quantify the extent of throats is to consider the location of wetting fluid at a particular capillary pressure. During both drainage and imbibition, it is common to find throats filled with wetting phase while the neighbouring pore bodies are oil-filled. Therefore, the dividing surface between pore bodies and throats can often be well represented by the fluid interface. Of particular help here is the covering radius transform (CRT) (Hilpert and Miller 2001), whose isosurfaces coincide with the interface between fluid phases at a particular hydraulic radius, for a contact angle of zero degrees. However, the CRT alone is not sufficient, since the CRT cannot distinguish constrictions – i.e. throats – from crevices, so throat volumes allocated using this measure alone would include crevices far away from the throat constriction. We add information on the location of the constrictions by supplementing the CRT with a

function which, for each voxel in the pore, contains the Euclidean distance to the throat constriction of interest. The throat is formed by growing out from the constriction, accessing progressively increasing values of the combined CRT-distance function. The growth stops when the maximum CRT value within the throat exceeds a threshold which is determined by a user-specified parameter called the throat volume factor. If this threshold is chosen to be the pore radius, then the throat will grow to completely fill the pore body, whereas if it is chosen to be the throat radius, then the throats will contain only a single layer of voxels.

Our rather complicated method for allocating volume to throats on the basis of local geometry contrasts with the approach of Oren and Bakke (1998) who use a very simple, if somewhat arbitrary formulation which determines a throat length from the ratio between the throat and pore radius. This formula will tend to allocate more volume than our algorithm to wide, low aspect ratio throats.

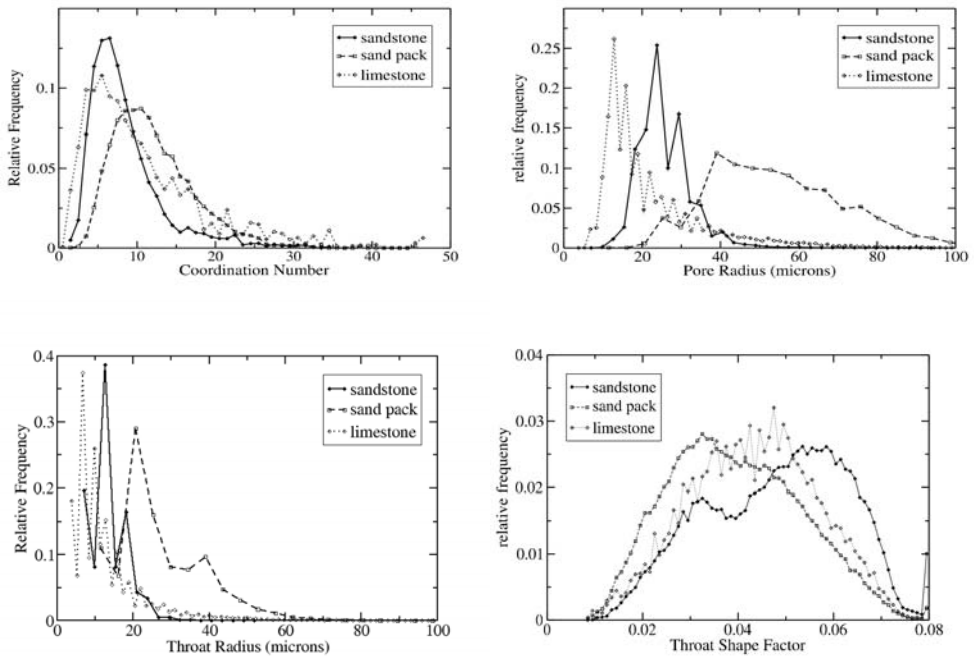

Fig 4: *Distributions of properties of the generated networks. Top left: coordination number. Top right: pore radius. Bottom left: throat radius. Bottom right: throat shape factor distribution.*

Throat shape factors depend on the pore-partitioning alone, being calculated from the throat cross section at the narrowest constriction using the dimensionless ratio between perimeter squared and area (Mason and Morrow 1991). Since the narrowest constriction isn't, in general, planar, the interface is projected onto its plane of best fit, and the throat extent on this plane is determined using two dimensional alpha-shapes. Additionally, as a consequence of pore merging, two pores may be connected by more than one throat. The interface between such pores will consist of more than one disconnected component. We treat multiple components by separately summing the perimeters and areas of all

components before taking their ratio. Throat shape factors calculated in this way lie between 0 and $1/4\pi$ (~0.08), with an equilateral triangle being 0.048. There is no single way to extend this formulation to calculate the shapes of three dimensional pore bodies. We have chosen the most natural extension, which is surface area/volume$^{2/3}$, and scaled so that it too fits in the same range as the throat shape factor. Fig. 4 shows the structural details of the generated network.

SINGLE PHASE PROPERTIES: VOXEL vs. NETWORK BASED

In this section we compare the single phase flow properties of voxel-based image data to those calculated on equivalent networks of the same image volume. The image based permeability calculations are based on a lattice-Boltzmann (LB) method (Arns et al 2004), and are currently limited to volumes of 400^3 voxels. Calculations are performed on subsets of the full tomographic image volume and an effective permeability for the full volume is estimated using the renormalization technique of Green & Paterson (2006). Network based permeability calculations are performed using the method described in Oren et al (1998) and Patzek and Silin (2001).

Table 2. *Permeabilities at Varying Scales: Image vs. Network*

Type	Size	# of pores	k_{image} (mD)	$k_{network}$ (mD)
Castlegate sandstone	200^3	673	3110	4003
	400^3	5133	2972	3214
	800^3	39862	2962	3001
unconsolidated	250^3	701	40549	60212
	500^3	5118	41641	40114
	1000^3	39055	41609	37985
limestone	480^3	1826	12852	25426
	960^3	13798	11534	10594

Castlegate Sandstone: Fig 5(a) compares image- and network-based calculations of permeability on subsets of the Castlegate. Image based calculations were performed on over one hundred different 200^3 subsets and then upscaled to 400^3 and 800^3, while the networks were directly generated on all image sizes. The equivalent network at 200^3 comprises approximately 700 pores; at 800^3 it has 40,000. A throat volume factor of 0.4 was used, resulting in ~12% of the pore volume being allocated to throats. We observe that the network calculations exhibit more scatter, and higher permeability (~30% higher) than the direct image-based value at 200^3. The average image based permeability is k_{image}=3.1 Darcy. This compares with a network model based permeability of $k_{network}$=4.0 Darcy. Comparisons at larger scales (400^3, 800^3) shows much better agreement between image and network (Fig. 6(b) & Table 2), with the difference at 800^3 being less than 2%.

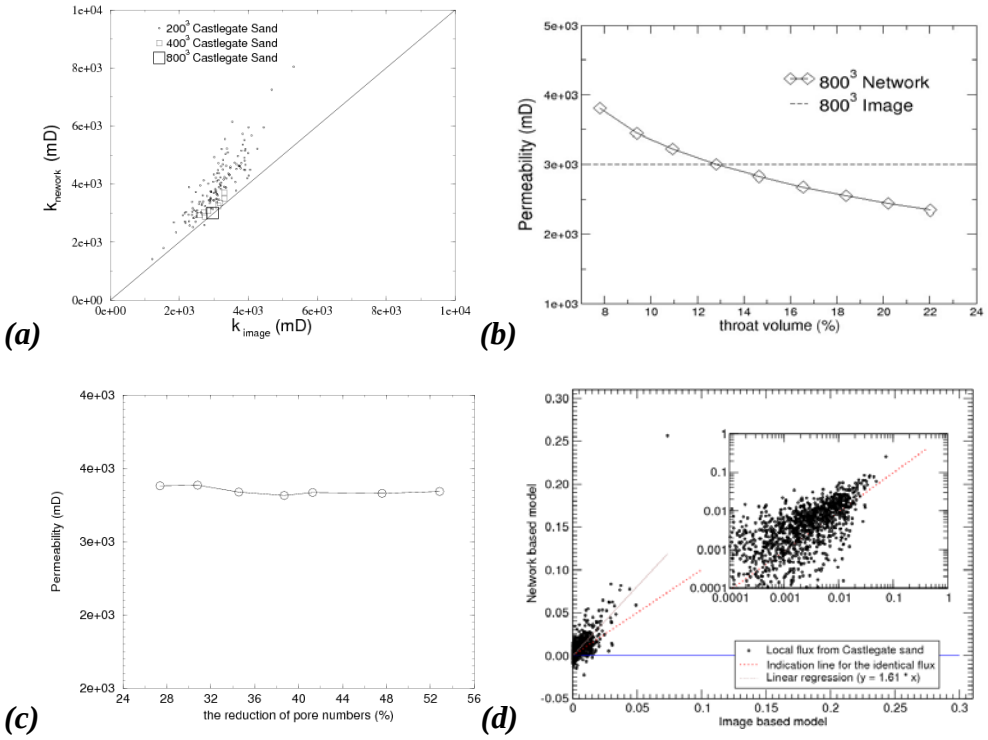

Fig. 5: *Castlegate sandstone data. (a) Comparison of image based (LB) and network permeability predictions, showing many different image subsets and different image sizes (200^3, 400^3, 800^3). Network data at the small scale overestimates the image based result. (b) Effect of throat volume factor on the resultant network permeability at 800^3. (c) Effect of pore merging on network permeability for 200^3 subvolume. (d) Comparison of the two methods' estimate of local flux between all internal pores of a single 200^3 subset.*

We also consider the sensitivity of network permeability to the free parameters in the network generation. Fig.5(b) shows the dependence of network model computed permeability on the throat volume factor. As expected, for smaller throat volumes the network permeability overestimates the image based value. For larger throat volumes the opposite trend is observed. The network and image based permeabilities agree when around 12% of volume in throats, corresponding to a throat volume factor of 0.4. The sensitivity to throat length is largely a consequence of the method traditionally used to calculate conductance (Patzek and Silin 2001), which assumes that the throat is a prism, i.e. that its radius is the minimum constriction radius for its entire length. Clearly, the conductance of any particular throat will be inversely proportional to its length if this expression is used. A better model would allow the throat radius to vary along its length. Fig. 5(c) shows the effect of pore merging on the overall prediction of permeability on a small network. Permeability is insensitive to pore merging for this homogeneous sandstone even at the small subset size of 200^3.

Fig. 5(d) compares the *local* flow rates in individual pores for the image and network model. At this time we can only make this comparison on relatively small systems (200^3). We note slightly larger local flow rates for the network compared to the image.

This is consistent with the result shown in Fig. 5(a). We observe significant scatter in the local flow rates but the overall agreement is reasonable.

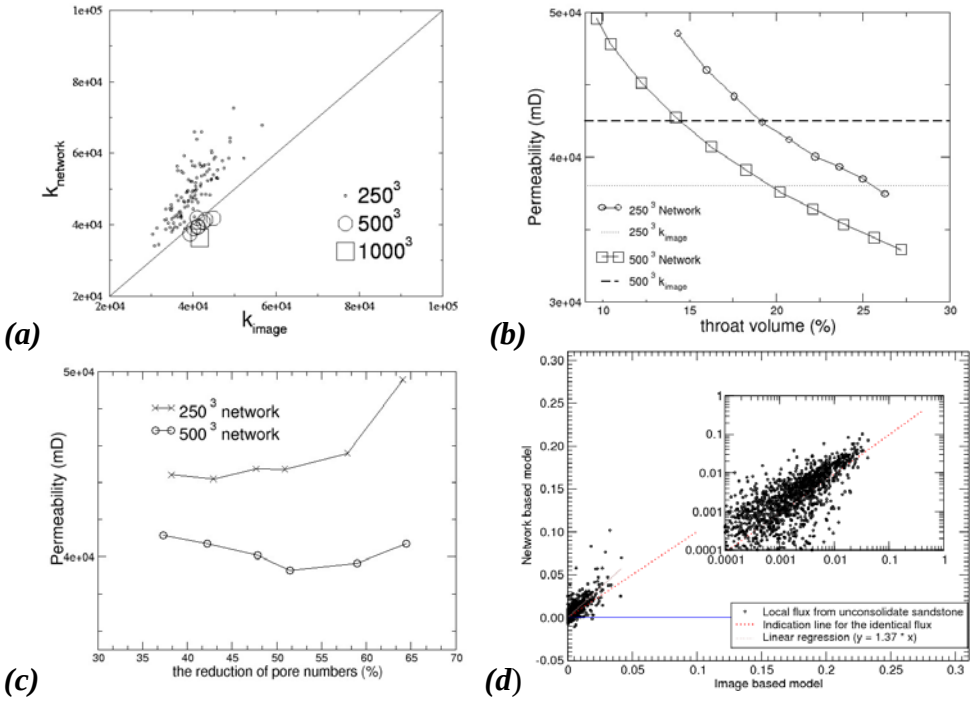

Fig. 6: *Unconsolidated sand pack. (a) Comparison of permeability on image and equivalent networks at different image sizes (250^3, 500^3, 1000^3); comparisons at the larger scale are in good agreement. (b) Effect of throat volume factor on the resultant network permeability. (c) Effect of pore merging on network permeability. (d) Comparison of local fluxes.*

Unconsolidated sand: Image and network based calculations of permeability are compared on 250^3, 500^3 and 1000^3 voxel subsets of the unconsolidated sandstone (comprising 700, 5000 and 39000 pores respectively) in Fig. 6(a) and Table 2. At the smallest scale the network model permeability is ~50% larger than the image based result. Again, the shape factor for each pore and throat is used from the image and the throat volume factor used is 0.4. The larger samples display greatly improved agreement. In Fig. 6(b) we plot the variation in the network permeability with variation in the throat volume factor. The best match is observed for a throat volume factor of 0.3. The effect of pore merging is shown in Fig. 6(c). Pore merging has some effect at the small scale but minimal effect for the larger scales. Local flux comparisons are shown in Fig 6(d), again showing that over-estimation of permeability appears to be broadly distributed throughout the network at 250^3.

Limestone: Due to the heterogeneity of this sample, image and network based calculations of permeability are compared at larger scales, 480^3 and 960^3 voxels, comprising 1800 and 14000 pores respectively. The results are summarized in Fig. 7(a) and Table 2. At the smaller scale the network model permeability is ~100% larger than

the image based result. The result for larger sample sizes is within 10%. In Fig. 7(b) we plot the variation in the network permeability with variation in the throat volume factor. An excellent match is observed for the throat volume factor of 0.4. The effect of pore merging is shown in Fig. 7(c). Again, pore merging has some effect at 480^3 but minimal effect on the larger scales. Fig. 7(d) shows the local flux comparisons at 300^3 and the reasonable agreement is observed, although the large scatters suggest the existence of heterogeneity and imply the need of large sample for the transport property calculation.

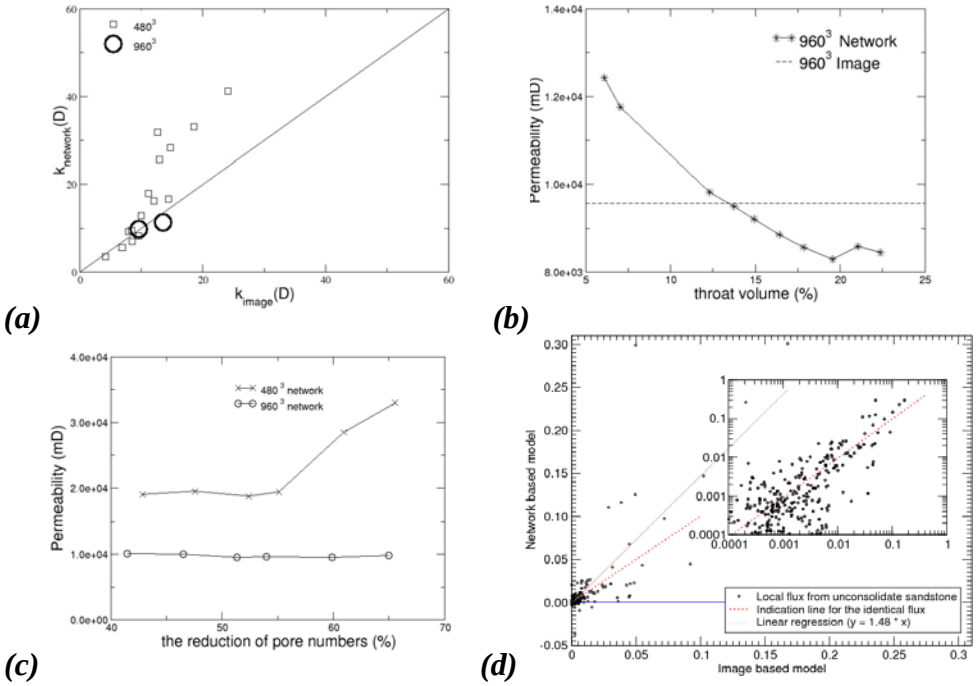

Fig. 7: Mt Gambier limestone (a) Comparison of permeabilities. (b) Effect of throat volume factor. (c) Effect of pore merging (d) Comparison of local fluxes.

MULTI-PHASE PROPERTIES: VOXEL vs. NETWORK BASED

A major advantage of network models over direct computations on images to estimate macroscopic properties is their ability to model the effect of wetting films in the crevices of the pore space (Bekri et al. 2003). Consequently, network models have been widely used to determine relative permeability and electrical resistivity (Blunt et al. 2002, Man and Jing 2002 and references within). Although wetting films play a crucial role in simulating laboratory-measured behaviour, particularly electrical resistivity, it is not clear that the assumptions of simple shape-factors and continuity of films between pores and the adjoining throats provides an adequate description of film behaviour in real rocks.

Berkowitz and Hansen (2001), using microtomographic images of Fontainebleau sandstone and a simulated annealing technique to find the minimum interfacial energy distribution at different saturations for strongly wetting conditions, suggest that wetting

films, at length scales greater than the resolution of the instrument (~ 5 microns) do not maintain continuity throughout the imaged volume. Although wetting films which may exist in corners and features below this resolution (surface roughness) would provide continuity, their effect on conductivity and resistivity would be considerably smaller that for the imaged thicker films. Network models, for similar wetting conditions, length scales and capillary pressures to those investigated by Berkowitz and Hansen (2001), would implicitly assume that films remain connected.

We investigate the continuity of the wetting phase for strongly wetting conditions at low saturations directly on the imaged pore space using the previously discussed covering radius transform (CRT). The image resolution is similar to that in the study of Berkowitz and Hansen (2001) - 2 to 3 microns. The isosurfaces of the CRT are a good approximation for the distribution of the wetting fluid in drainage at quasi-static conditions. To quantify the connectivity of the corner, or crevice wetting phase we compute isosurfaces and the corresponding wetting phase saturations at different capillary pressures. We then test each throat in the network to determine if it transports wetting fluid. We do this using a pore partitioning and the following algorithm: consider a throat that connects neighbouring pores, pore A and pore B. First determine whether the wetting phase connects across pore A from pore B to at least one other of A's neighbour pores. If so, and if the wetting phase also connects across A from B, then the throat is considered open to flow. At lower wetting phase saturations, some throats are closed, causing a reduction in the coordination number of the pores they connect. The average coordination number is thus a useful measure of the continuity of the wetting fluid at low wetting fluid saturations where continuity is dominated by wetting phase in corners.

Fig. 8(a) shows the average wetting phase network effective coordination number as a function of saturation for the consolidated, unconsolidated and outcrop carbonate cores discussed previously. For the consolidated Castlegate sandstone the wetting fluid begins to disconnect significantly at a wetting fluid saturation of approximately 0.4 becoming increasingly disconnected with decreasing saturation. The unconsolidated plug maintains connectivity down to a saturation of approximately 0.2. The Mt. Gambier carbonate outcrop displays intermediate behaviour. The present results are in qualitative agreement with those of Berkowitz and Hansen (2001) for Fontainebleau sandstone. The effect of crevice wetting disconnection on resistivity and relative permeability is the subject of ongoing study.

Fig. 8(b) shows computed resistivity index curves for a diluted cubic network with triangular pore and throat shapes and increasing fractions of randomly distributed circular shaped pores and throats. Since circular cross-sections cannot accommodate corner wetting phase at any capillary pressure, increasing their fraction in the network mimics the effects of reducing wetting phase connectivity in the network. The computations are for a primary drainage (strongly water wet conditions) where the only mechanism for corner wetting phase disconnection is the a priori introduction of circular cross-sections.

The effect of corner wetting phase disconnection is dramatic, with a wide range of behaviour possible. A similarly wide range of behaviour has been demonstrated by the introduction of wettability effects (Man and Jing 2002).

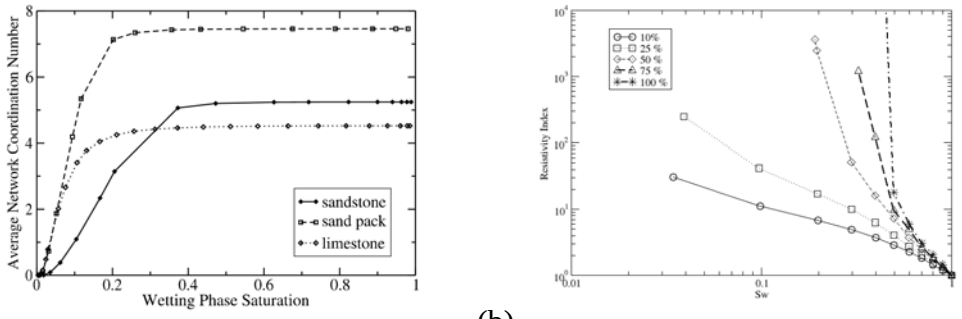

(a) (b)

Fig. 8: (a) Network average coordination number as a function of wetting phase saturation. (b) Resistivity index as a function of wetting phase saturation, calculated on a simple network model, with corner wetting phases in differing fractions of throats disconnected.

CONCLUSIONS

On the basis of detailed comparisons of permeability and wetting fluid continuity computed directly on 3D images of the pore space and network models extracted from the images we make the following conclusions:

1. Image based permeabilities and those computed from equivalent network models are in good agreement provided the volume of rock imaged is sufficiently large.

2. Pore partitioning can be achieved using the watershed transform with only a single free parameter, the degree of pore merging. Although this parameter has a significant effect on the characteristics of the extracted network, the effect on the computed permeability is small.

3. Partitioning into both pores and throats demands at least one additional free parameter – the throat volume factor – which has a significant effect on the computed permeability for the network model. For the partitioning criteria used in the present work a throat volume factor of approximately 0.4 provides good agreement with image based calculations for the three rocks under consideration.

4. An image based investigation of the connectivity of the wetting phase shows that corner wetting phase becomes increasingly disconnected as the wetting phase saturation is reduced. This may have a significant effect on electrical resistivity at lower wetting phase saturations.

ACKNOWLEDGEMENTS

The authors acknowledge the member companies of the Digital Core Consortium for their support. We thank the A.N.U. Supercomputing Facility and the Australian Partnership for Advanced Computing for very generous allocations of computer time.

REFERENCES

1. Arns, C.H., M.A. Knackstedt, W.V. Pinczewski, and N. Martys: "Virtual permeametry on microtomographic images." *J. Petroleum Sci. and Eng.* (2004) **45**, 41-46.
2. Bekri S, Howard J, Muller J, and Adler P.M. "Electrical Resistivity Index in Multiphase Flow through Porous Media", *Transport in Porous Media* (2003) **51**, 41-65.
3. Berkowitz B. and Hansen D.P., "A Numerical Study of the Distribution of Water in Partially Saturated Porous Rock", *Transport in Porous Media*,(2001) **45**, 303-319.
4. Blunt M, Jackson M.D, Piri M, Valvatne Per. H., "Detailed physics, predictive capabilities and macroscopic consequences for pore network models of multiphase flow", *Advances in Water Resources* (2002) **25**, 1069-1089.
5. Green, C.P. and Paterson, L., "Analytical three-dimensional renormalization for calculating effective permeabilities", *Transport in Porous Media*,(2006)**68**,237-248.
6. Hilpert, M. and C. T. Miller, "Pore-morphology based simulation of drainage in a totally wetting porous media", *Advances in Water Resources* (2001) **24**(2), 157-177.
7. Lindquist, W.B, A. Venkatarangan, J. Dunsmuir, T-f. Wong "Pore and throat size distributions measured from synchrotron X-ray tomographic images of Fontainebleau sandstone", *Journal of Geophyical Research* (2000) **105**, 509-527.
8. Man H.N. and Jing X.D., "Network modelling of mixed wettability on electrical resistivity, capillary pressure and wettability indices", *Journal of Petroleum Science and Engineering* (2002) **33**, 101-122.
9. Mason, G and N. R. Morrow, "Capillary behaviour of a perfectly wetting liquid in irregular triangular tubes", Journal of Colloid and Interface Science (1991), **141**, 262.
10. Oren, P. –E., S. Bakke, O. Arntzen "Extending predictive capabilities to network models", *SPE Journal* (1998) paper 38880.
11. Patzek, T.W. And Silin, D.B., "Shape factor and hydraulic conductance in noncircular capillaries. I. One-phase creeping flow", *J. of Colloid Interface Science*. (2001) **236**: 295-304.
12. Russ, John C.: "The Image Processing Handbook, 5th edition", CRC Press (2007), 493-496.
13. Sheppard, A. P, R. M. Averdunk, R. M. Sok, V. B. Robins, C. H. Arns, M. Saadatfar, "Analysis of rock microstructure using high-resolution X-ray tomography", Annual Symposium of the Society of Core Analysts (2006), Norway, paper SCA2006-26 .
14. Sheppard, A.P, H, Averdunk, R. M. Sok "Improved pore-network extraction methods", Annual Symposium of the Society of Core Analysts (2005), Canada, paper SCA2005-20.